Review of Scientific Instruments

A transportable Paul-trap for levitation and accurate positioning of micron-scale particles in vacuum for laser-plasma experiments

Cite as: Rev. Sci. Instrum. **89**, 013302 (2018); https://doi.org/10.1063/1.4995955
Submitted: 13 July 2017 . Accepted: 02 November 2017 . Published Online: 03 January 2018

T. M. Ostermayr, J. Gebhard, D. Haffa, D. Kiefer, C. Kreuzer, K. Allinger, C. Bömer, J. Braenzel, M. Schnürer, I. Cermak, J. Schreiber, and P. Hilz

A transportable Paul-trap for levitation and accurate positioning of micron-scale particles in vacuum for laser-plasma experiments

T. M. Ostermayr,[1,2,a)] J. Gebhard,[1] D. Haffa,[1] D. Kiefer,[1] C. Kreuzer,[1] K. Allinger,[1] C. Bömer,[3] J. Braenzel,[4] M. Schnürer,[4] I. Cermak,[5] J. Schreiber,[1,2] and P. Hilz[1]
[1]*Ludwig-Maximilians-Universität München, Fakultät für Physik, 85748 Garching, Germany*
[2]*Max-Planck-Institut für Quantenoptik, 85748 Garching, Germany*
[3]*European XFEL, 22869 Schenefeld, Germany*
[4]*Max-Born-Institut, 12489 Berlin, Germany*
[5]*CGC Instruments, Hübschmannstr. 18, 09112 Chemnitz, Germany*

(Received 13 July 2017; accepted 2 November 2017; published online 3 January 2018)

We report on a Paul-trap system with large access angles that allows positioning of fully isolated micrometer-scale particles with micrometer precision as targets in high-intensity laser-plasma interactions. This paper summarizes theoretical and experimental concepts of the apparatus as well as supporting measurements that were performed for the trapping process of single particles. https://doi.org/10.1063/1.4995955

I. INTRODUCTION

Electrodynamic quadrupole traps[1] have been a viable tool in diverse fields of science ever since their invention.[2,3] While traps for single ions and atoms are widespread in research, traps for macroscopic particles comprised of more than 10^8 atoms are used in fewer research branches.[4–6] Here we present an electrodynamic quadrupole trap that was designed for applications requiring isolated micrometer-sized particles with μm position-accuracy in vacuum while providing large optical access to the particle.

The specific motivation for this development is their use in high-intensity laser-plasma experiments as a target system, where a tightly focused laser-pulse interacts with an isolated target.[7] Experiments require large optical access for both the high-intensity laser that is focused into the trap center via a large-numerical-aperture focusing optics and for the diagnostics of laser-plasma interaction products. The resulting ultrashort and intense X-ray, ion, and electron bursts are expected to have important applications in physics and medical research. In this respect, theoretical work and simulations have shown that isolated targets could have important advantages over bulk foil targets, particularly concerning the maximum energy of energetic ions as well as their energy distribution and source size distribution.[8–14] Other very active areas of research are studies of warm dense matter (WDM) and the isochoric heating of material, where so-called reduced mass targets (RMT) are often used for better comparability of experiments with simulations and analytical models.[15–18]

Mechanical mounting of these targets is often accomplished by spider silk[19] (0.1–1 μm diameter) or glass capillaries and other small structures[19–21] (1–10 μm diameter). This limits the size of the actual target to diameters larger than 10 μm. To avoid the necessity of a target mount, droplet sources are a viable tool.[22–24] They are inexpensive and support high repetition rates (>kHz). On the other hand, the necessity to synchronize the target with the laser, the gaseous environment around the target, and the restrictions on target material are eminent drawbacks. Also, the accessible target diameter is limited to 8-60 μm. The quest for even smaller targets has led to the development of gas cluster targets.[25–27] Clusters with diameters up to several 100 nm diameter can be formed in expanding mixtures of gas. Considering these clusters as targets, they are limited in available target material, and they are randomly distributed within the gaseous environment which unavoidably fills (or exceeds) the focal volume. In consequence, several thousand cluster targets typically interact with the laser pulse in a single shot, limiting the isolated target character in such experiment.

Generally, materials near the target, including the target-mount, neighboring targets, and background gas, contribute significantly to the laser-target interaction.[21,25,28] Albeit being tiny in scale and mass, they have profound implications even for larger-scale plasmas used in inertial confinement fusion.[29]

This paper summarizes theoretical and experimental concepts of the transportable and adaptable Paul-trap apparatus as well as the outline of one possible implementation in a laser-plasma experiment. The system can provide targets of any solid material with diameters currently ranging from 500 nm to 50 μm. It thereby closes the existing gap in target diameter between cluster and droplet targets and enables scans across a large diameter-range using a single experimental setup. The novel target is truly isolated and avoids any kind of nearby structures or background gas, while its position is defined on the μm level. Measurements on single levitating particles are presented to demonstrate reproducibility, stability, and precision of particle positioning.

II. THEORETICAL CONCEPTS

The idea of electrodynamic traps is the levitation of charged particles by means of the electric field despite the

a)Author to whom correspondence should be addressed: tobias.ostermayr@physik.lmu.de

Earnshaw theorem[30] stating that this is unachievable for a purely electrostatic field. Time-dependent electric fields are able to produce ponderomotive wells[1] and enable the construction of so-called Paul-traps of which different kinds exist.

The electric potential in a linear Paul-trap can be written in terms of time t and two spacial dimensions x and y as $\Phi(\vec{x},t) = V\ \cos\ \Omega t \cdot (x^2 - y^2)/r_0^2$, where V is the amplitude of the AC voltage applied to the trap electrodes, Ω is the angular drive frequency, and r_0 is the effective radius of the trap. To generate this kind of potential accurately, electrode-surfaces must ideally lie on equipotential surfaces of such an electric field, i.e., the ideal trap has to be constructed of four infinitely sized hyperbolically shaped electrodes around the trap center that are infinitely extended in the third spatial dimension z (i.e., do not produce any electric field in that direction). For the realization of a trap in such a linear setup, the axial confinement has to be solved by additional measures, e.g., additional electrodes. The equation of motion of a particle in this potential reads as $M\mathrm{d}^2\vec{x}/\mathrm{d}t^2 = -Q\vec{\nabla}\Phi(\vec{x})$, where Q and M are the charge and the mass of the particle, respectively. They take the form of Mathieu differential equations for x and y, which are well characterized with respect to their solutions.[31] Two general types of solutions exist:[32] stable solutions remain limited in their spatial extent and can thus be identified with a trapped particle, while unstable solutions diverge in spatial extent and correspond particles that leave the trap within a short time. This distinction is based on a single number, the q-parameter, calculated from trap and particle properties as $q = 4QV/Mr_0^2\Omega^2$. The range $0 < q < 0.908$ results in stable trajectories. For larger q, the solution is unstable, and particles collide with the electrodes or leave the trap after gaining kinetic energy from the electric field. The parameter q is also a practical measure for the adiabaticity of the system: for parameters $q < 0.3$, the system can be assumed to be adiabatic,[33] meaning that the energy in the macromotion is conserved and the particle is not kinetically heated by the temporally varying electric field. In the following, we consider only this adiabatic regime of operation.

The particle trajectory is then a superposition of two parts:[34] a fast oscillatory term, the so-called micromotion x_{mic}, which is directly excited by the fast alternating electric field, and a slower motion x_{mac}, referred to as macromotion, which can be regarded as the net-motion after averaging over one trap-voltage oscillation period.

The macromotion x_{mac} can be described as a simple harmonic oscillator,

$$\ddot{x}_{mac} + x_{mac}\omega_{\mathrm{sec}}^2 = 0, \tag{1}$$

oscillating with the so-called secular frequency $\omega_{\mathrm{sec}} = q\Omega/\sqrt{8}$. For this kind of motion, one can find a corresponding quasistatic pseudopotential by integration that reads

$$U_p(x_{mac}) = \frac{1}{4}qV\frac{x_{mac}^2}{r_0^2}. \tag{2}$$

This potential is usually referred to as pseudopotential or effective potential, since it describes the effective force acting on the particle, averaged over the oscillation-period of the electric field. It thereby provides important insight into the strength of the confinement of a particle in the trap.[35]

In our setup, we use a trap with four cylindrical rods as AC electrodes. In contrast to infinitely sized hyperbolically shaped electrodes, this provides a larger optical access to the trap center. The downside is that the cylindrical rod geometry gives rise to higher order potential terms with the next higher contributing orders being the 12-pole and the 20-pole.[36] Our arrangement also deviates significantly from the optimized cylindrical geometry[37,38] with $r_{rod}/r_0 = 1.145\,11$ where the 12-pole term vanishes. In contrary to the ideal quadrupole field, the resulting equations of motion are coupled in coordinates, and the particle motion is anharmonic, i.e., the motion frequency is amplitude dependent.[39] It is further known that higher order multipoles lead to unstable trajectories for some otherwise stable values of q (i.e., there appear unstable regions within $0 < q < 0.908$) due to resonant heating of the particle.[40–42] However, effects of higher-order potentials are mostly discussed in context of the effective trapping volume for storing large ion clouds and their implications for precision measurements.[43] In our approach, we minimize their practical influence by several means: First, we operate the trap with $q < 0.4$, i.e., in a region where only very high order instabilities exist.[42] Second, the target is supposed to levitate very close to the trap center for our studies, where higher order contributions are naturally minimized as they scale with higher orders of distance from the trap center, than the quadrupole term does. The difference of the quadrupole term in the real trap to that of a trap with ideal geometry can be characterized simply by means of a modified (effective) inner radius[43] r_0^{eff} within the classical framework of equations.

The confinement in the third spatial dimension in our trap is achieved by the application of additional DC potentials via end-cap electrodes. This leads to an additional frequency component of the particle motion ω_z along the z coordinate. Additional anharmonic fields arise but vanish in the trap center—where we aim to confine the particle—due to symmetry. They are thus neglected in this simplified discussion.

The preparation of trapped particles in the trap center without significant residual motion requires damping of the initial particle motion. The amplitude of the micromotion is proportional to the amplitude of the local electric field and thus vanishes in the trap center. In consequence, assuming negligible gravitational and electrostatic forces, an efficient damping of the harmonic macromotion amplitude is sufficient for the target positioning. To that end, we use the electric feedback field $E(x_{mac})$ reacting to the electro-optically measured and electronically filtered particle trajectory x with a proper phase-shift, modifying the harmonic macromotion described by Eq. (1) to that of a damped harmonic oscillator, thereby efficiently damping the macromotion after few tens to thousands of oscillation periods.

III. EXPERIMENTAL CONCEPTS

A. Test setup

In order to develop the Paul-trap for laser plasma experiments, a compact minimum-setup was developed which is

sketched in Fig. 1. A central part thereof is a chamber that allows evacuation to pressures down to 10^{-6} mbar. Typical laser-plasma experiments operate at pressures below 10^{-5} mbar in order to avoid effects of the gaseous environment on the high-intensity laser and to ensure proper detection of charged particle beams from the laser-plasma interaction, preventing effects on their charge state by the limited mean-free-path. The test chamber emulates such environment. The Paul-trap itself is depicted in Fig. 2. It consists of four cylindrical copper rods with diameters of 5 mm arranged around the trap center at geometric distance $r_0 = 8.1$ mm, leading to an effective inner radius[43] of $r_0^{\text{eff}} = 8.7$ mm. In return, the setup provides a large optical access to the trap center, i.e., allows us to use large-numerical-aperture optics as usually employed with ultrahigh-intensity lasers. The rod distance and diameters can be adjusted to suit the specific setup and can accommodate even f/1 optics in the current configuration.

Two round copper slabs with diameters of 3 mm serve as endcaps located at a distance of 10-20 mm in between each other to create the potential in the z-dimension. All AC electrodes and endcaps are positioned with respect to each other in precision-manufactured ceramics seats, which also isolate them electronically from each other. Each AC electrode as well as both endcaps is connected to their individual voltage supply. The setup features frequencies $\Omega/2\pi$ up to 5 kHz and voltages V up to 3 kV for the AC electrodes and DC voltages up to 450 V for the endcaps.[44]

Above the center of the trap, a particle reservoir is mounted which is filled with few milligrams commercial sample of monodisperse spherical particles.[45] The loading mechanism of the trap works similar to a salt shaker: upon mechanical actuation of the reservoir, several particles fall through a hole of 100 μm diameter into the trap. The charging of the particles is performed via an ion beam that is crossing their path. The ion gun was built at Tectra[46] delivering ion currents of several

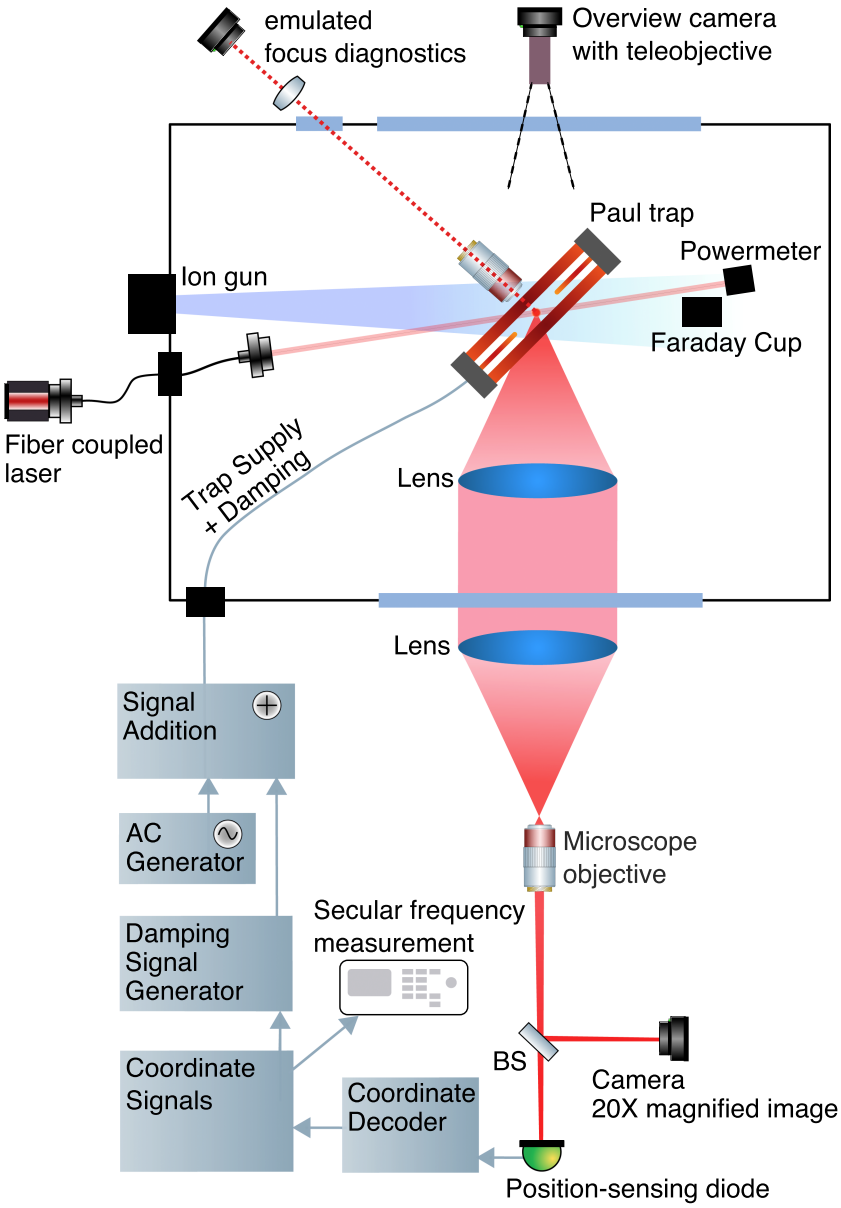

FIG. 1. The minimum Paul-trap test-setup comprises a vacuum chamber, the trap and connected power supplies, an ion gun to charge the target particles, a laser to illuminate target particles, and the optical measurement and feedback setup.

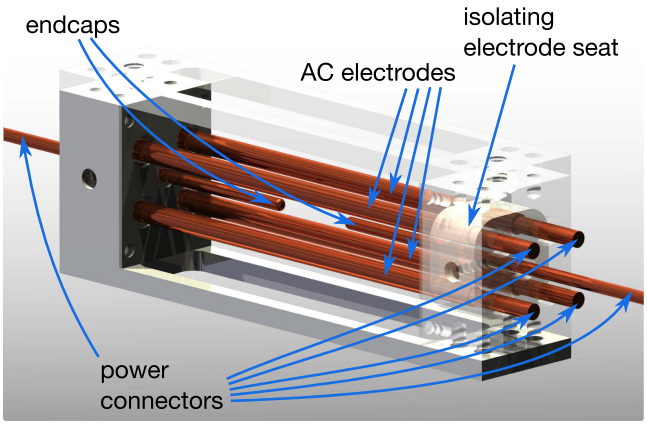

FIG. 2. The Paul-trap, consisting of four AC electrodes and two DC endcaps. All electrodes are positioned in precision manufactured isolating ceramics seats.

10 nA/mm^2 at up to 5 keV ion energy. The current is permanently monitored by a Faraday cup. The ion gun is supplied with an adjustable gas flow of air or helium which temporarily increases the pressure inside the chamber to 10^{-5}–10^{-4} mbar. Typically a few particles are trapped. By reducing the endcap voltages to a few volts before trapping, the Coulomb repulsion between trapped particles reliably and quickly pushes all but one particle out of the trap. After the initial trapping process, the ion gun is turned off, and the pressure is reduced to the lowest attainable value within a second. The endcap voltages are ramped up to their final voltage to ensure strong confinement in all dimensions. Overall, the initial trapping process takes around 10-30 s.

For the illumination of the particles, a 660 nm laser diode with a maximum output power of 50 mW is used. A maximum of 32 mW of this power was coupled into a single-mode fiber. Inside the vacuum chamber, a connected adjustable collimator lens is used to loosely focus the laser to a spot size between 0.25 and 1 mm FWHM (Full-Width at Half Maximum) in the center of the trap. The stray light from the target is collected by three independent imaging systems for different purposes. The overview camera monitors the trap and reservoir systems during the initial trapping process. A 20× microscope, referred to as "emulated focus diagnostics," is used to produce micrometer-resolution videos of the particle trajectory and to quantify the position stability of the damped particle. It resembles the microscope used later in experiments for target-focus alignment. The main optical system is comprised of two identical 4″ lenses with an F-number of 1 to create a 1:1 image outside of the chamber. This image is magnified by a 20× objective and divided by a beamsplitter onto (a) a camera that monitors the particle position, ultimately until the high-power laser-shot is fired. At this time, the focus diagnostics used to establish the laser-target overlap must have been removed from the laser-beam path to avoid its destruction. And (b) onto a position-sensing diode (PSD) which tracks the center-of-mass motion of the particle's image. The two electric signals from the PSD provide information about the 2D-projection of the particle motion onto the PSD plane (i.e., vertical and horizontal directions). The analog bandwidth of the coordinate detection is around 10 kHz. This provides sufficient headroom for measuring the typical particle motion in the sub-kHz range. From these time-domain signals, the frequency of the particle motion was derived via frequency analysis of one coordinate-signal by means of an FFT algorithm. The secular frequency provides the highest peak in the frequency spectrum. The coordinate signals are also used for electric damping of the particle motion. The methodology will be presented in more detail in a separate paper. Here we describe just the key idea: The particular coordinate signal was phase-shifted and applied as an additional voltage to the corresponding trap electrodes. The purpose was to provide an electric field that is proportional to the negative particle velocity, thus to generate a damping term in the particle's equation of motion.[44,48] The result was an effective damping of the particle motion without the necessity of any gas agent typically used to damp particle oscillations.

Note that the 2D projection on the PSD contains information about the particle's motion along all the three major axes of the trap. The vertical PSD signal contains information on the motion in the vertical dimension of the trap only, which occurs at the secular frequency ω_{sec}. The horizontal signal is composed of all motion in horizontal coordinates of the trap. The first major axis in this plane is taken along the endcaps (z-coordinate), where particle motion occurs at the frequency ω_z. The second axis in this plane is perpendicular to the z–axis, where the secular motion occurs at the frequency ω_{sec}. Resulting damping voltages for the horizontal coordinates contain both damping signals. Naturally, the trapped particle reacts stronger to the properly phased resonant part of the damping voltage in each dimension, than it reacts to the potentially heating, but non-resonant and non-phase-matched part, which is meant for the respective other coordinate. Thus, the damping can become effective in all three spatial dimensions, despite measuring only two of them.

We want to highlight some choices that were made in the concept. One key feature is the charging by an ion gun, which enables orders of magnitude larger charge-to-mass ratios of the particles as compared with charging mechanisms that were used in previous concepts, e.g., charging by discharge.[49] Due to the relation of kinetic particle energy to the potential energy in the trap $E_{kin}(0) = QU_p(x_{max})$, the residual amplitude x_{max} decreases with higher charge, for a given kinetic energy. The most important parts of the concept are the optical setup and the optoelectronic damping which enable experiments with well positioned targets at high-vacuum conditions, such that we do not rely on buffer gas for particle positioning.[49] This is important to ensure that the high-power laser and diagnostics for the laser plasma interactions are not affected by a gaseous environment. Moreover, the setup allows variable implementations in various target chambers, e.g., in that the distance between both identical lenses is adjustable to fit specific chamber geometries. The system must collect the small amount of stray light created by tiny target particles. Since only the center-of-mass of the particle's image is tracked by the PSD, which does not necessarily need to be in focus, we opted for the earlier mentioned large aperture f/1 lenses with comparably small depth of focus (~1–2 μm). The potential disadvantage of limited depth of focus is more than

compensated by the enhanced efficiency in collecting the light from the particle. For example, the high-numerical-aperture lens of the optical system allows us to collect several nW power from a 1 μm particle. For even smaller particles down to 100 nm, an optional image-intensifier with a gain of 10^3 can be placed in the position of the 1:1 image outside of the vacuum chamber, to artificially increase the PSD signal-to-noise ratio. The fiber-coupled laser is brought into the vacuum chamber through a vacuum feedthrough, which—together with the light-collecting powermeter—serves to reduce any kind of stray-light other than that from the particle itself. We identified this as crucial. It also allows us to position the illuminating source inside the chamber compact and variable to adapt to different laboratories.

B. Example setup in a laser plasma experiment

It is worth to briefly describe a possible implementation in a laser-plasma experiment, which exemplary is shown in Fig. 3. In order to protect optical components of the trap setup that are located close to focal planes of imaging systems, where stray-light from the high-power laser-plasma interaction can become particularly intense, we introduce fast mechanical shutters[50] to these beampaths. This concerns both the fiber-coupled illumination laser and the imaging system used for the electronic feedback-loop. The closing-time of our shutters is specified as 6 ms across 25 mm, such that imaging systems are saved from the high-power laser shot just about one secular

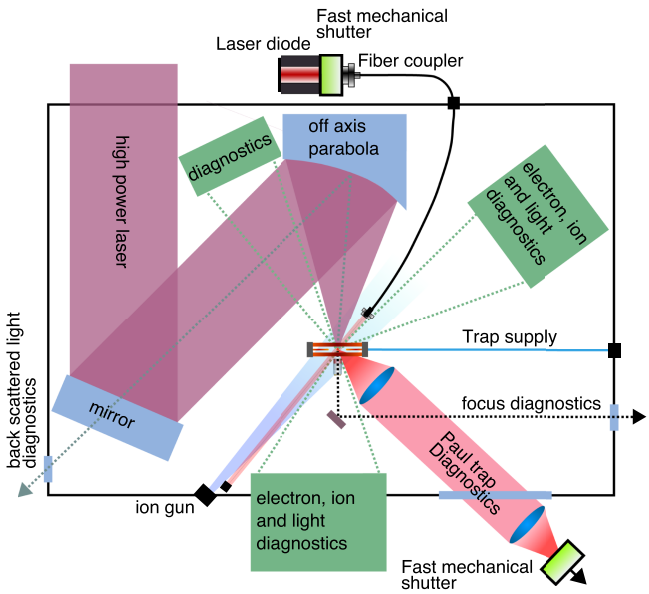

FIG. 3. Implementation of the Paul-trap setup in a laser-plasma experiment. The laser is folded once inside the target vacuum chamber and focused onto the levitating target by an off-axis parabolic mirror. For the adjustment of laser-target overlay, the focus diagnostic microscope is installed consisting of a microscope objective and a mirror to guide the image out of the vacuum chamber, where the image is produced by a tube lens and a camera. The optical path of this microscope is sketched by a black dotted line. Several detectors for electrons, ions, and x-rays can be installed in the plane of laser propagation, sketched in green, together with the angles that remain unoccupied indicated by green dotted lines. The backscatter diagnostic is sketched in dotted gray. It makes use of the fact that the parabolic mirror efficiently recollects light that is backscattered from the target. The turning mirror transmits a small portion of that light which is sufficient for a spectral analysis.

oscillation period before its arrival. We verified that this method and the time scale do not influence the relevant position accuracy. In experiments with up to 150 J laser energy, the stray-light coming off the high-power laser-target interaction did no harm to the first lens at a 4″ distance from the trap center. For higher laser energies, which might potentially damage this lens, the possibility exists to introduce the fast optical shutter earlier in the imaging system.

In addition to the equipment described in Sec. III A, the setup needs to accommodate the equipment that is inherent to the laser-plasma experiment. That is the high-intensity laser itself, typically including a short focal-length focusing optic (off-axis parabolic mirror). The focus-diagnostics microscope that is routinely emulated in the test setup shown before is now used in the direction of laser propagation, downstream of the target-mount. It serves for fine adjustments, both of the high-power laser-focus and the three-dimensional laser-target overlap. This microscope can be moved out of the beam-path by motorized stages prior to full-power laser shots. During laser and target adjustments, a strongly attenuated version of the high-power laser is used. Furthermore, the laser plasma experiment requires diagnostics for interaction products such as energetic ion and electron bunches or photon pulses in a broad spectral range. In Fig. 3, we suggest a possible set of diagnostics that could consist of electron-, ion-, and X-ray spectrometers. We have also employed a diagnostic for the backscattered optical light (spatial and/or spectral information) that relies on the small amount of backscattered light that leaks through the turning mirror. More diagnostics are usually accommodated outside of the horizontal laser-plane.

IV. SELECTED MEASUREMENTS OF RELEVANT SINGLE PARTICLE PARAMETERS

A. Charge-to-mass ratio

The real-time tracking of the particle enables the measurement of the secular frequency. For this purpose, the PSD coordinate signal in the vertical dimension was measured for a 12-s long period in the time-domain. The power spectral density of the recorded motion was calculated via the discrete Fourier transformation of the time-domain signal and revealed the secular frequency as the dominant peak in the frequency domain. An example of such measurement is displayed in Fig. 4. During these measurements, the particle trajectory was adjusted to fill ~3/4 of the PSD field-of-view, corresponding to ~300 μm in the real space. All damping measures were turned off during the measurement. The peak could be unambiguously identified as the particle's secular frequency because it shifted according to the expectations when the trap-parameters (Ω, V) were changed. From the secular frequency, the charge-to-mass ratio Q/M and the physical strength of the confinement in the trap in terms of the pseudopotential can be inferred [using the known relation of q and ω_{sec} given in the theory section, the definition of U_p in Eq. (2) and the known trap parameters r_0, Ω, and V]. Both are strong indicators for the ability of the trap to accurately position a particle. In the following example, we demonstrate the method for a polystyrene

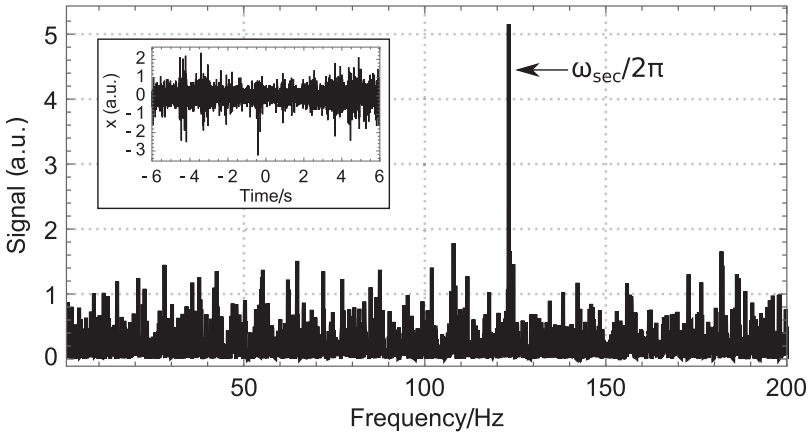

FIG. 4. Example of a trajectory measurement in the time-domain (inset) for the vertical PSD signal and corresponding power-spectral density (frequency measurement) via Fourier transformation of the time-domain signal.

target of 10 μm diameter. Figure 5 shows secular frequencies measured for six consecutively trapped particles with trap parameters $\Omega/2\pi$ = 1.1 kHz, V = 1.0 kV and r_0 as specified earlier. Error bars are inferred from the spectral width of the frequency peak and scaled up by a factor of 100 for better readability. The mean secular frequency is found as $\omega_{sec}/2\pi$ = 125 Hz, given as a black solid line, with a standard deviation of 9 Hz (indicated by the gray band). The example reveals a reproducible charge-to-mass ratio of 0.29 C/kg corresponding to a surface potential of the sphere of 288 V. The corresponding electric field at the particle surface of 58 MV/m is in the range of the dielectric strength of the material[51] of about 20 MV/m that is expected to limit the achievable particle charge.[48] At pressures of 10^{-6} mbar, the value stays constant for many hours.[4] The q-parameters are inferred close to 0.3. Consistency checks were performed by tuning q to the region where particle trajectories naturally become unstable (q = 0.908) by lowering the trap frequency. The particle trajectories consistently turned unstable and left the trap, for frequencies of 675 Hz > $\Omega/2\pi$ > 650 Hz, corresponding to $q \cong 0.908$.

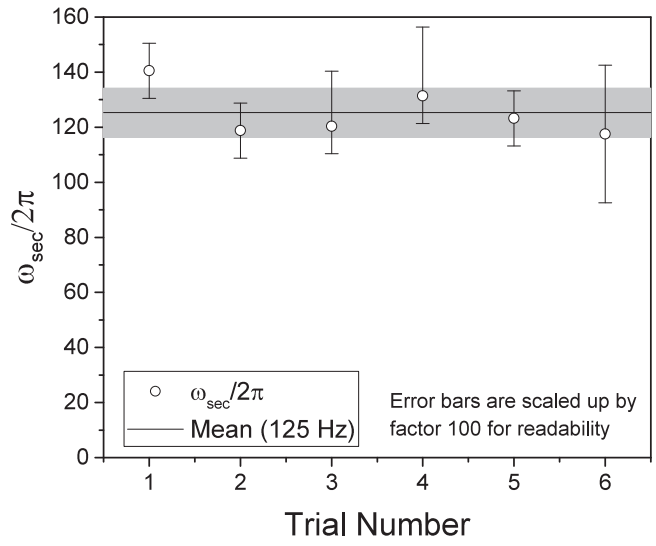

FIG. 5. Secular frequencies for particles trapped consecutively, measured at $\Omega/2\pi$ = 1100 Hz. The horizontal line shows the mean value of $\omega_{sec}^{mean}/2\pi$ = 125 Hz, and the gray band indicates the standard deviation. Error bars are inferred from the spectral width of single measurements and scaled by a factor 100 for readability. These measurements reveal the comparably small variation of secular frequencies and charge-to-mass ratios, demonstrating the overall stability of the charging mechanism.

From these measurements and the well-defined particle mass, it is also straightforward to retrieve the charge carried by the specific target. For $\omega_{sec}/2\pi$ = 125 Hz in the example, that is Q = 9.9(0.9) × 10^5 e. The specified error stems from the distribution of particle diameter in the employed sample, specified with 3% root-mean-square deviation. The trapped particle itself was comprised of 5 × 10^{13} hydrogen and carbon atoms, easily outnumbering the number of elementary charges brought onto it. For laser-plasma experiments, it is therefore valid to consider the trapped particle as unvaried from its original specification. The charge Q leads further to the potential energy QU_p = 69 MeV or 11 pJ evaluated at the distance r_0 from the trap center. This is more than an order of magnitude larger than the particle energy resulting from a free fall from a height of several cm and facilitates our straightforward trapping process in the first place. It shall be mentioned that this specific trap setup was not laid out or optimized by any means for high-resolution spectroscopic measurements. Still, the presented measurements and calculations serve to characterize particle and trap properties sufficiently well for our purpose. Thereby, a reliable, controlled, and stable trapping procedure was established as a basis for the trajectory damping and, ultimately, for laser-plasma experiments.

B. Residual motion

In the current mode of operation, solely relying on the opto-electronic damping in high-vacuum, the initial trapping process and the damping of the initial particle motion to its final residual amplitude take tens of seconds to several minutes, depending on particle composition, size, and initial conditions. The most important measurement for the practical usability of trapped particles as targets is the quality of the damping, quantified by the amplitude of the residual motion of a trapped particle. We measured the extent of the remaining particle motion using the emulated focus diagnostics. The 20-fold magnification allowed us to resolve the motion. For Fig. 6, we trapped a 10-μm diameter polystyrene particle at 1500 V, 1400 Hz rod voltage, and 250 V DC endcap voltage. We captured 12 900 frames with 70 μs exposure time each, at a frame-rate of 7.5 Hz. The exposure time is shorter than micro- and macromotion oscillation periods of the particle. From each image,

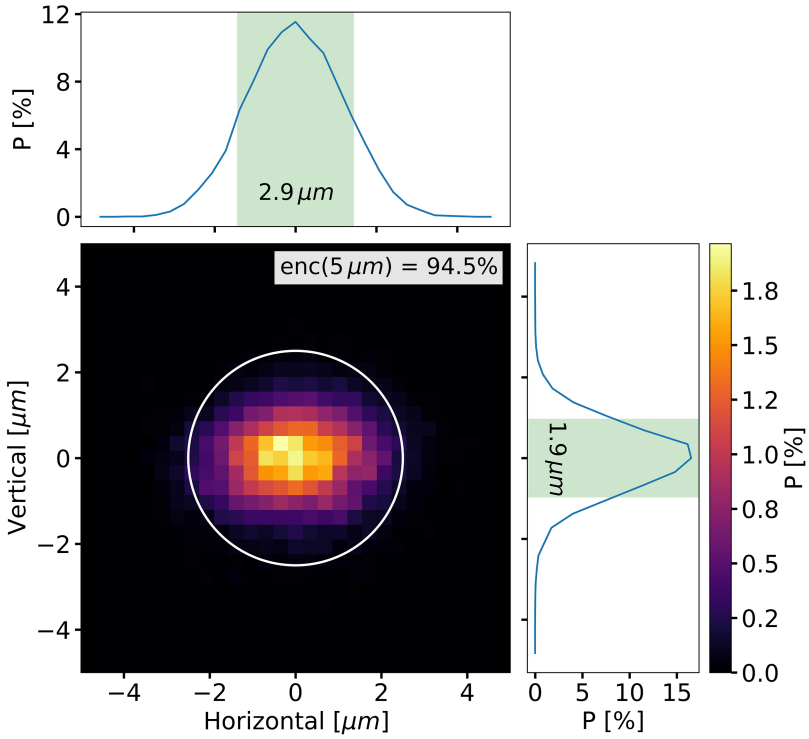

FIG. 6. Distribution of the tracked center of mass for a 10-μm diameter trapped polystyrene sphere imaged at 20-fold magnification. The camera exposure time of 70 μs for each frame recorded at 7.5 Hz was chosen short enough to resolve single points of the particles micro motion. The convoluted hit probability of a 5 μm FWHM laser-focus would be 94.5%. In particular, positioning is more accurate than typical laser-pointing jitters.

we determine the center of mass and plot the two-dimensional histogram of the occurrence of a specific particle position in Fig. 6. The Full-Width at Half Maximum (FWHM) of the motion is confined to 2.9 μm in the horizontal direction and 1.9 μm in the vertical direction. Once the particle is damped to such level of residual motion, it can stay confined for hours and longer. The white circle refers to the FWHM diameter of a typical high-power laser focus of 5 μm. From this, we can expect a hit-probability (defining hit with at least half-peak intensity interaction with the sphere center) of 94.5%. This estimate does not take into account pointing instabilities of typical large-scale high-power laser systems that are often of the order of their FWHM spot-size. We note that the presented center-of-mass tracking is the most straightforward and accurate method available to determine residual motion, since more direct methods (e.g., time-integrated imaging) are easily flawed by the particle motion along the microscope dimension (out of the image plane), and by the complex optical properties of transparent micro-particles, which can both lead to blurred images even for particles at rest.

The measurement in Fig. 6 was performed in our test-laboratory situated in the first floor of a laboratory and office building. Tables of the setup are built of solid aluminum structures and do not implement further damping techniques. It is noteworthy that measurements during general day-time at which the building is comparably populated are sensitively influenced by all kinds of vibrations caused by this population. Presented measurements regarding damping and stability were recorded in less populated times. For technical reasons, the majority of large laser systems are situated in ground-level or basement floors, often taking special care for vibration stability. This comes to the advantage of our setup in its designated environment.

V. CONCLUSIONS AND OUTLOOK

We have presented theoretical and experimental concepts as well as measurements for single trapped particles to demonstrate the operational capability of a novel electrodynamic quadrupole trap. Spherical polymer particles with diameters ranging from 500 nm to 50 μm as well as tungsten particles with diameters up to 10 μm have been trapped and positioned to comparable precision with this setup already. The system provides this uniquely wide range of target parameters in an isolated and well-controlled way and has been successfully implemented at high-intensity laser facilities at the Max-Born Institute (MBI, Berlin), the PHELIX laser (GSI, Darmstadt), and the Texas Petawatt Laser (TPW, UT Austin)[7] in experiments investigating laser-driven ion acceleration from micro-plasmas. The MBI experiment was historically the first one and relied on buffer-gas damping at 10^{-4} mbar, while all other experiments used the active feedback damping without buffer-gas. Figure 7 shows exemplary data obtained with these laser systems. A manuscript discussing further results is currently under review for publication. The hit probability of laser shots using 5–10 μm FWHM laser foci on the target has constantly been larger than 50% and was limited by laser-pointing jitters. This reconfirms the usefulness of the target system for laser-microplasma investigations.

Current developments of the setup cover two major pillars. First, an improvement of the current maximum repetition rate of the 1 trapping process (and laser-shot) per 15 min is pursued via automation of the complete initial trapping sequence. In the presented state of the system, there are three manual actions required for each initial trapping of a particle, which slows down the overall performance: the power

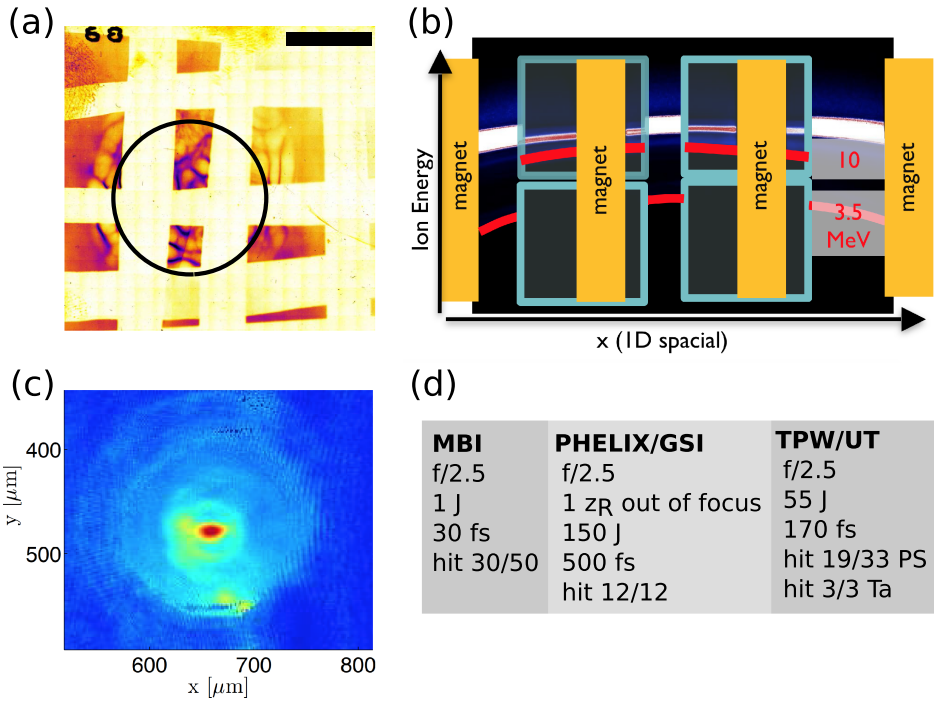

FIG. 7. Exemplary data obtained in three different experiments. (a) Nuclear track detector used at MBI when shooting at a 1.9 μm polymer particle. The detector was positioned in laser propagation direction at 50 mm distance to the target. The scale bar corresponds to 10 mm. The detector exclusively records ions after they passed different thickness of aluminum filters. (b) Typical raw-data recorded by an ion wide angle spectrometer at the PHELIX laser, for a shot onto a 1 μm polymer target. The red lines signify iso-energy lines for protons according to cutoffs produced by 100 μm aluminum filters (covering the complete detector) and 1 mm CR39 filters (cyan squares). (c) Time integrated plasma self-emission of a 7 μm tantalum target recorded at TPW. (d) Laser parameters and the hit-ratio (hit/total shot number) for each experiment (specifying "hit" as a shot that produced reasonably measurable signal in each diagnostics). PS refers to polystyrene targets Ta refers to tantalum targets.

on/off of the ion gun, together with the gas-flow adjustment through it, the actuation of the particle reservoir mechanism, and the ramping of end-cap voltages after the initial trapping process. As the experiment areas are usually controlled for radiation safety, any such human interaction directly at the system costs time to re-establish the safety protocol. However, all these actions can be automated in a similar way like the remaining part of the present system, such that a single push-button can remotely trigger the full trapping sequence. Once this development has been completed, the system itself will support much larger repetition rates than the current 1 shot per 15 min. The first cornerstone for this is the imaging system, which practically requires the adjustment of the laser-target overlap only once by use of the focus-diagnostics. Once this overlap is established, the reproducible positioning of targets in the focus can be achieved equally well by means of the Paul trap optical system. Unlike the focus-diagnostics, this setup does not require physical motion of optical elements before and after the laser engagement and is therefore compatible with a higher repetition rate. The second cornerstone is the demonstrated reproducibility of the charge-to-mass ratio for consecutively trapped particles. This allows us to operate the system at constant parameters for a given choice of a particle-sample, thereby reducing time and effort for consecutive trapping processes. The third and last cornerstone is the implementation of a hybrid damping-scheme combining buffer-gas damping for the early stage (shortly after trapping) and active damping for the final damping. This can reduce overall damping time considerably, since the currently deployed active damping is rather ineffective in the early stage, i.e., with initial particle trajectories exceeding the field of view of the optical system. We anticipate a fundamental limit of the repetition rate for our target-system at around 1 Hz, as we typically require hundreds of oscillation periods to damp the particle trajectory, and secular frequencies are typically in the few-hundred Hz range. Similarly, charging times will realistically stay in the second range. This would suffice to make full use of next generation laser systems, including the 1 Hz, 3 PW ATLAS3000 laser currently being built at the Center for Advanced Laser Applications (CALA) in Garching. Besides that, we consider the presented system as a unique tool to study and identify ideal target parameters at a given laser system and for a given purpose from the very broad supported target-parameter range. This allows one to invest reasonably into a more narrow-range solution developed specifically aiming at high repetition rates (e.g., droplet targets or cluster targets) or to develop new solutions, if the desired parameter-set is unavailable by other high-rep means. The necessity and requirements of such investment (or development) into narrow parameter-range targets will ultimately be driven and dictated by the aimed-at real-world application.

The second pillar of current work concentrates on the preparation of isolated non-spherical particles such as graphene nanoplatelets[52] as targets. In addition to the damping of their trajectory, they require controllable orientation in the trap with respect to the high-power laser. This will open

a completely new realm of plasma parameters to be studied, without strings attached. Simulations promise significant potential for usable X-ray and proton beam generation from such target.[9,53,54]

ACKNOWLEDGMENTS

This work was supported by the DFG via the Cluster of Excellence Munich-Centre for Advanced Photonics (MAP) and Transregio SFB TR18. T.M.O. acknowledges support from IMPRS-APS. J.G. acknowledges support from Hanns-Seidel-Stiftung. This work has been carried out within the framework of the EUROfusion Consortium and has received funding, through the ToIFE, from the European Union's Horizon2020 research and innovation program under Grant Agreement No. 633053. P.H. and T.M.O. acknowledge the support of Dr. Johannes Wulz with the LMU physics design team and Rolf Oehm with the LMU physics workshop in laying out, prototyping, and constructing the trap. We also acknowledge J. Pavlů and I. Richterová from Charles University in Prague for their shared experience and their support with spare parts that are impossible to get elsewhere. T.M.O., P.H., and J.S. acknowledge the support of scientific and technological staff at the MBI Berlin, the UT Austin (Gilliss Dyer, Mikael Martinez, Michael E. Donovan, Erhard Gaul, Joe Gordon, Edward McCary, Craig Wagner, Michael Spinks, and Manuel Hegelich) and the GSI Darmstadt (Bernhard Zielbauer, Udo Eisenbarth, Stefan Götte, Dirk Reemts, Sabine Kunzer, Florian Wagner, and Vincent Bagnoud) in conducting the experiments with their high-power lasers.

[1] W. Paul, in *Nobel Lectures, Physics 1981-1990*, edited by T. Frängsmyr and G. Ekspong (World Scientific Publishing Co., Singapore, 1993).
[2] *Physics with Trapped Charged Particles*, edited by M. Knoop, N. Madsen, and R. C. Thompson (Imperial College Press, London, 2014).
[3] G. Werth, V. N. Gheorghe, and F. Major, *Charged Particle Traps II*, Springer Series on Atomic, Optical, and Plasma Physics Vol. 54 (Springer Berlin Heidelberg, 2009).
[4] J. Pavlů, I. Richterová, Z. Němeček, J. Safrankova, and I. Cermak, Faraday Discuss. **137**, 139 (2007).
[5] J. Spann, M. Abbas, C. Venturini, and R. Comfort, Phys. Scr. **T89**, 147 (2001).
[6] M. Abbas, P. Craven, J. Spann, D. Tankosic, A. LeClair, D. Gallagher, E. West, J. Weingartner, W. Witherow, and A. Tielens, Astrophys. J. **614**, 781 (2004).
[7] T. M. Ostermayr, D. Haffa, P. Hilz, V. Pauw, K. Allinger, K.-U. Bamberg, P. Böhl, C. Bömer, P. R. Bolton, F. Deutschmann, T. Ditmire, M. E. Donovan, G. Dyer, E. Gaul, J. Gordon, B. M. Hegelich, D. Kiefer, C. Klier, C. Kreuzer, M. Martinez, E. McCary, A. R. Meadows, N. Moschüring, T. Rösch, H. Ruhl, M. Spinks, C. Wagner, and J. Schreiber, Phys. Rev. E **94**, 033208 (2016).
[8] W. Yu, H. Xu, F. He, M. Y. Yu, S. Ishiguro, J. Zhang, and A. Y. Wong, Phys. Rev. E **72**, 046401 (2005).
[9] S. S. Bulanov, A. Brantov, V. Y. Bychenkov, V. Chvykov, G. Kalinchenko, T. Matsuoka, P. Rousseau, S. Reed, V. Yanovsky, D. W. Litzenberg, K. Krushelnick, and A. Maksimchuk, Phys. Rev. E **78**, 026412 (2008).
[10] T. Kluge, W. Enghardt, S. D. Kraft, U. Schramm, K. Zeil, T. E. Cowan, and M. Bussmann, Phys. Plasmas **17**, 123103 (2010).
[11] J. Limpouch, J. Psikal, A. Andreev, K. Y. Platonov, and S. Kawata, Laser Part. Beams **26**, 225 (2008).
[12] F. Peano, R. A. Fonseca, and L. O. Silva, Phys. Rev. Lett. **94**, 033401 (2005).
[13] F. Peano, F. Peinetti, R. Mulas, G. Coppa, and L. O. Silva, Phys. Rev. Lett. **96**, 175002 (2006).
[14] M. Murakami and M. Tanaka, Phys. Plasmas **15**, 082702 (2008).
[15] P. Neumayer, H. J. Lee, D. Offerman, E. Shipton, A. Kemp, A. L. Kritcher, T. Döppner, C. A. Back, and S. H. Glenzer, High Energy Density Phys. **5**, 244 (2009).
[16] J. Myatt, W. Theobald, J. A. Delettrez, C. Stoeckl, M. Storm, T. C. Sangster, A. V. Maximov, and R. W. Short, Phys. Plasmas **14**, 056301 (2007).
[17] H. Nishimura, R. Mishra, S. Ohshima, H. Nakamura, M. Tanabe, T. Fujiwara, N. Yamamoto, S. Fujioka, D. Batani, M. Veltcheva, T. Desai, R. Jafer, T. Kawamura, Y. Sentoku, R. Mancini, P. Hakel, F. Koike, and K. Mima, Phys. Plasmas **18**, 022702 (2011).
[18] W. Theobald, K. Akli, R. Clarke, J. A. Delettrez, R. R. Freeman, S. Glenzer, J. Green, G. Gregori, R. Heathcote, N. Izumi *et al.*, Phys. Plasmas **13**, 043102 (2006).
[19] B. A. Brinker, J. M. Cavese, J. R. Miller, S. G. Noyes, S. Sheble, and L. T. Whitaker, J. Vac. Sci. Technol., A **1**, 941 (1983).
[20] A. Henig, D. Kiefer, M. Geissler, S. G. Rykovanov, R. Ramis, R. Hörlein, J. Osterhoff, Z. Major, L. Veisz, S. Karsch, F. Krausz, D. Habs, and J. Schreiber, Phys. Rev. Lett. **102**, 095002 (2009).
[21] K. Zeil, J. Metzkes, T. Kluge, M. Bussmann, T. Cowan, S. Kraft, R. Sauerbrey, B. Schmidt, M. Zier, and U. Schramm, Plasma Phys. Controlled Fusion **56** 084004 (2014).
[22] T. Sokollik, M. Schnürer, S. Steinke, P. V. Nickles, W. Sandner, M. Amin, T. Toncian, O. Willi, and A. A. Andreev, Phys. Rev. Lett. **103**, 135003 (2009).
[23] S. Karsch, S. Düsterer, H. Schwoerer, F. Ewald, D. Habs, M. Hegelich, G. Pretzler, A. Pukhov, K. Witte, and R. Sauerbrey, Phys. Rev. Lett. **91**, 015001 (2003).
[24] S. Ter-Avetisyan, M. Schnürer, P. V. Nickles, M. Kalashnikov, E. Risse, T. Sokollik, W. Sandner, A. Andreev, and V. Tikhonchuk, Phys. Rev. Lett. **96**, 145006 (2006).
[25] S. Ter-Avetisyan, B. Ramakrishna, R. Prasad, M. Borghesi, P. V. Nickles, S. Steinke, M. Schnürer, K. I. Popov, L. Ramunno, N. V. Zmitrenko, and V. Yu Bychenkov, Phys. Plasmas **19**, 073112 (2012).
[26] T. Ditmire, J. Zweiback, V. Yanovsky, T. Cowan, G. Hays, and K. Wharton, Nature **398**, 489 (1999).
[27] Y. Fukuda, A. Y. Faenov, M. Tampo, T. A. Pikuz, T. Nakamura, M. Kando, Y. Hayashi, A. Yogo, H. Sakaki, T. Kameshima, A. S. Pirozhkov, K. Ogura, M. Mori, T. Z. Esirkepov, J. Koga, A. S. Boldarev, V. A. Gasilov, A. I. Magunov, T. Yamauchi, R. Kodama, P. R. Bolton, Y. Kato, T. Tajima, H. Daido, and S. V. Bulanov, Phys. Rev. Lett. **103**, 165002 (2009).
[28] A. Morace, C. Bellei, T. Bartal, L. Willingale, J. Kim, A. Maksimchuk, K. Krushelnick, M. S. Wei, P. K. Patel, D. Batani, N. Piovella, R. B. Stephens, and F. N. Beg, Appl. Phys. Lett. **103**, 054102 (2013).
[29] S. R. Nagel, S. W. Haan, J. R. Rygg, M. Barrios, L. R. Benedetti, D. K. Bradley, J. E. Field, B. A. Hammel, N. Izumi, O. S. Jones, S. F. Khan, T. Ma, A. E. Pak, R. Tommasini, and R. P. J. Town, Phys. Plasmas **22**, 022704 (2015).
[30] S. Earnshaw, Trans. Cambridge Philos. Soc. **7**, 97 (1842).
[31] J. Meixner and F. Schäfke, *Mathieusche Funktionen und Sphäroidfunktionen*, 1st ed., Die Grundlehren der Mathematischen Wissenschaften in Einzeldarstellungen Vol. LXXI (Springer Berlin Heidelberg, 1954).
[32] F. Major, V. N. Gheorghe, and G. Werth, *Charged Particle Traps*, Springer Series on Atomic, Optical, and Plasma Physics Vol. 37 (Springer Berlin Heidelberg, 2005).
[33] S. Stenholm, Rev. Mod. Phys. **58**, 699 (1986).
[34] H. Dehmelt, *Radiofrequency Spectroscopy of Stored Ions I: Storage*, Advances in Atomic and Molecular Physics, Vol. 3 (Academic Press, 1968), pp. 53–72.
[35] R. F. Wuerker, H. Shelton, and R. V. Langmuir, J. Appl. Phys. **30**, 342 (1959).
[36] D. R. Denison, J. Vacuum Sci. Technol. **8**, 266 (1971).
[37] I. E. Dayton, F. C. Shoemaker, and R. F. Mozley, Rev. Sci. Instrum. **25**, 485 (1954).
[38] G. Lee-Whiting and L. Yamazaki, Nucl. Instrum. Methods **94**, 319 (1971).
[39] K. Blaum, C. Geppert, P. Müller, W. Nörtershäuser, E. Otten, A. Schmitt, N. Trautmann, K. Wendt, and B. Bushaw, Int. J. Mass Spectrom. **181**, 67 (1998).
[40] Y. Wang, J. Franzen, and K. Wanczek, Int. J. Mass Spectrom. Ion Processes **124**, 125 (1993).
[41] M. Vedel, J. Rocher, M. Knoop, and F. Vedel, Appl. Phys. B **66**, 191 (1998).
[42] R. Alheit, C. Hennig, R. Morgenstern, F. Vedel, and G. Werth, Appl. Phys. B **61**, 277 (1995).

[43]J. Pedregosa, C. Champenois, M. Houssin, and M. Knoop, Int. J. Mass Spectrom. **290**, 100 (2010).
[44]CGC Instruments, Chemnitz, Germany.
[45]See http://www.microparticles-shop.de for Microparticles GmbH, Berlin, retrieved 30 June 2017.
[46]See www.tectra.de for Tectra GmbH, retrieved 25 February 2016.
[47]See http://www.sitek.se/pdf/psd/s2-0003-2l10_su7.pdf/ for Sitek, PSD Model: 2L10-SU7, last checked 12.10.2017.
[48]I. Cermak, "Laboruntersuchung elektrischer aufladung kleiner staubteilchen," Ph.D. thesis, Ruprecht-Karls-Univeristät, Heidelberg, 1994.
[49]T. Sokollik, T. Paasch-Colberg, K. Gorling, U. Eichmann, M. Schnürer, S. Steinke, P. V. Nickles, A. Andreev, and W. Sandner, New J. Phys. **12**, 113013 (2010).
[50]See https://www.uniblitz.com/products/vs25/ for Uniblitz, retrieved 17 June 2017.
[51]C. Harper, *Modern Plastics Handbook* (McGraw-Hill, 2000).
[52]B. E. Kane, Phys. Rev. B **82**, 115441 (2010).
[53]T. P. Yu, Z. M. Sheng, Y. Yin, H. B. Zhuo, Y. Y. Ma, F. Q. Shao, and A. Pukhov, Phys. Plasmas **21**, 053105 (2014).
[54]T.-P. Yu, A. Pukhov, Z. M. Sheng, F. Liu, and G. Shvets, Phys. Rev. Lett. **110**, 045001 (2013).